

RESEARCH LETTER

10.1002/2014GL061943

Key Points:

- Objective front ID applied to historical and RCP8.5 CMIP5 simulations
- Compared to ERA-Interim, models represent frequency and strength of fronts well
- Projections show decrease in front frequency in NH and poleward shift in SH

Supporting Information:

- Readme
- Table S1
- Figure S1
- Figure S2
- Figure S3
- Figure S4

Correspondence to:

J. L. Catto,
jennifer.catto@monash.edu

Citation:

Catto, J. L., N. Nicholls, C. Jakob, and K. L. Shelton (2014), Atmospheric fronts in current and future climates, *Geophys. Res. Lett.*, *41*, 7642–7650, doi:10.1002/2014GL061943.

Received 20 SEP 2014

Accepted 16 OCT 2014

Accepted article online 20 OCT 2014

Published online 10 NOV 2014

Atmospheric fronts in current and future climates

J. L. Catto¹, N. Nicholls¹, C. Jakob², and K. L. Shelton¹

¹School of Earth, Atmosphere and Environment, Monash University, Clayton, Victoria, Australia, ²Centre of Excellence for Climate Systems Science, School of Earth, Atmosphere and Environment, Monash University, Clayton, Victoria, Australia

Abstract Atmospheric fronts are important for the day-to-day variability of weather in the midlatitudes. It is therefore vital to know how their distribution and frequency will change in a projected warmer climate. Here we apply an objective front identification method, based on a thermal front parameter, to 6-hourly data from models participating in Coupled Model Intercomparison Project phase 5. The historical simulations are evaluated against ERA-Interim and found to produce a similar frequency of fronts and with similar front strength. The models show some biases in the location of the front frequency maxima. Future changes are estimated using the high emissions scenario simulations (Representative Concentration Pathway 8.5). Projections show an overall decrease in front frequency in the Northern Hemisphere, with a poleward shift of the maxima of front frequency and a strong decrease at high latitudes where the temperature gradient is decreased. The Southern Hemisphere shows a poleward shift of the frequency maximum, consistent with previous storm track studies.

1. Introduction

Atmospheric fronts are important for providing the day-to-day variability of weather in the midlatitudes. They are associated with a large proportion of global rainfall [Catto *et al.*, 2012], are often associated with extreme rain events [Catto and Pfahl, 2013], and can cause damaging flood events [Pitt, 2008]. They also bring a large proportion of the growing season rainfall to southern parts of Australia [Pook *et al.*, 2006, 2012].

Since the first conceptual models of frontal systems were developed [Bjerknes and Solberg, 1922], fronts have been used on weather maps to indicate the position of cloud and rain bands. The structure of fronts and the weather associated with them have been widely reported using case studies [e.g., Browning and Monk, 1982] and intensive observational campaigns [e.g., Joly *et al.*, 1999].

Only recently have studies looked at long-term climatologies of fronts on global or hemispheric scales. Berry *et al.* [2011a] and Simmonds *et al.* [2011] applied automated front identification techniques to large-scale reanalysis data. Simmonds *et al.* [2011] used a method identifying shifts in the meridional component of the wind to identify fronts in the Southern Hemisphere. Berry *et al.* [2011a] applied the objective front identification methodology of Hewson [1998], a method employing a thermal front parameter, to produce a global climatology of fronts and expanded it in Berry *et al.* [2011b] to investigate recent trends in front frequency. These two methods were found to compare well in their identification of fronts over south west Western Australia [Hope *et al.*, 2014]. Indeed, automated synoptic identification methods have now reached maturity [Neu *et al.*, 2013; Ulbrich *et al.*, 2013].

The importance of fronts at global and regional scales means that it is vital to know how their spatial distribution and frequency of occurrence may change in the future. A number of studies have suggested that the Southern Hemisphere storm tracks are likely to shift poleward in the future, and the frequency of cyclones will decrease slightly [Chang *et al.*, 2013; Grieger *et al.*, 2014]. On the other hand, projected changes in the Northern Hemisphere storm tracks are not as clear as a large variety of influences contribute to the response of the storm tracks to a warming climate. Among them are the relative cooling in the North Atlantic due to the slowdown of the meridional overturning circulation, and the Arctic amplification of the global temperature increases [Catto *et al.*, 2011; Woollings *et al.*, 2012]. Future changes in front frequency will be strongly related to changes in the storm tracks. One goal of the present study is to investigate the potential future changes in global front distributions and to relate these to changes in the storm tracks seen in other studies.

In order to have confidence in projections of front frequency, first the climate models must be able to represent its present-day distribution. The unprecedented availability of data from phase 5 of the Coupled Model Intercomparison Project (CMIP5) [Taylor *et al.*, 2012] at high temporal resolution (6-hourly) means that front identification methods can be applied to a number of climate models. There have been a number of recent studies evaluating the representation of the midlatitude storm tracks in the CMIP5 models [e.g., Zappa *et al.*, 2013a; Colle *et al.*, 2013] and other models [e.g., Chang *et al.*, 2013]. These studies found that many of the models underestimate the number of cyclones in the Northern Hemisphere midlatitude storm tracks [Zappa *et al.*, 2013a; Colle *et al.*, 2013] and that the storm tracks exhibit an equatorward bias in both hemispheres [Chang *et al.*, 2013]. Catto *et al.* [2013] performed the first evaluation of atmospheric fronts in a single atmosphere-only climate model (The Australian Community and Climate Earth System Simulator; ACCESS) [Bi *et al.*, 2013]. The present study aims to expand this work to evaluate the representation of fronts in a number of state-of-the-art climate models.

2. Method and Tools

The objective front identification method of Berry *et al.* [2011a], which follows the same techniques as Hewson [1998], has been applied to 6-hourly reanalysis and model data. This method identifies frontal points using a thermal front parameter [Renard and Clarke, 1965] based on the 850 hPa wet-bulb potential temperature. The thermal front parameter field is masked using a threshold of $-8 \times 10^{-12} \text{ km}^{-2}$ [Berry *et al.*, 2011a] then frontal points are identified where the gradient of the thermal front parameter is zero and a line-joining algorithm is used to link the frontal points into contiguous fronts. The fronts are then separated into warm, cold, and quasi-stationary categories depending on their frontal speed and direction.

Here data from the European Centre for Medium-Range Weather Forecasting reanalysis data set, ERA-Interim [Dee *et al.*, 2011], are extracted every 6 hours at 1.5° resolution. The temperature and specific humidity at 850 hPa are used to calculate the wet-bulb potential temperature, and the zonal and meridional components of the 850 hPa wind are used to separate the fronts into their different categories. The front identification is applied to the data interpolated to 2.5° resolution (as in Catto *et al.* [2012]) for the period 1980–2005 (for consistency with the model data), and the front locations are kept on the 2.5° grid. This data set provides an observationally constrained data set against which to evaluate the model data.

We apply the same front identification method to the data from a number of models contributing to the CMIP5 [Taylor *et al.*, 2012]. These 18 models from 11 modeling centers are listed in Table S1 in the supporting information and are chosen from the complete set of CMIP5 models based on the availability of the required 6-hourly data from both the present-day and future simulations. To evaluate the representation of the fronts in the current climate, the years 1980–2005 from the historical simulations are used. Future scenarios are derived from the Representative Concentration Pathway 8.5 (RCP8.5) experiment for the period of 2080–2100. This extreme future scenario is used to investigate the response to the largest of the RCP climate forcings. The 6-hourly instantaneous temperature, specific humidity, meridional and zonal wind are extracted on 850 hPa from one arbitrarily chosen run of each of the models for the historical and RCP8.5 simulations. The data are interpolated onto the same 2.5° grid as the ERA-Interim data before the front identification is applied, and then the fronts are kept on the same 2.5° grid as those from ERA-Interim.

The front frequency is calculated as the percentage of days (from 00Z to 18Z) on which a front is present in a grid box. This has been presented for an annual average, with some seasonal figures presented in the supporting information. To investigate the biases in the models and the future changes over the main storm track regions, we compute the zonally averaged front frequency for three different regions: the North Atlantic (80°W to the Greenwich Meridian); the North Pacific (130°E to 130°W); and the Southern Ocean (all longitudes). The strength of the fronts is measured by the wet-bulb potential temperature gradient across the front.

3. Evaluating Historical Simulations

Figure 1 shows the front frequency for ERA-Interim (Figure 1a), the multimodel mean (Figure 1b), and the difference between the multimodel mean and ERA-Interim (Figure 1c). The multimodel mean shows maxima in the front frequency in the major storm track regions of the Northern Hemisphere (NH) and Southern Hemisphere (SH) and looks very similar to the ERA-Interim structure and magnitude of the front frequency. In the North Atlantic region the maximum front frequency is over 30%, and in the North Pacific it is over

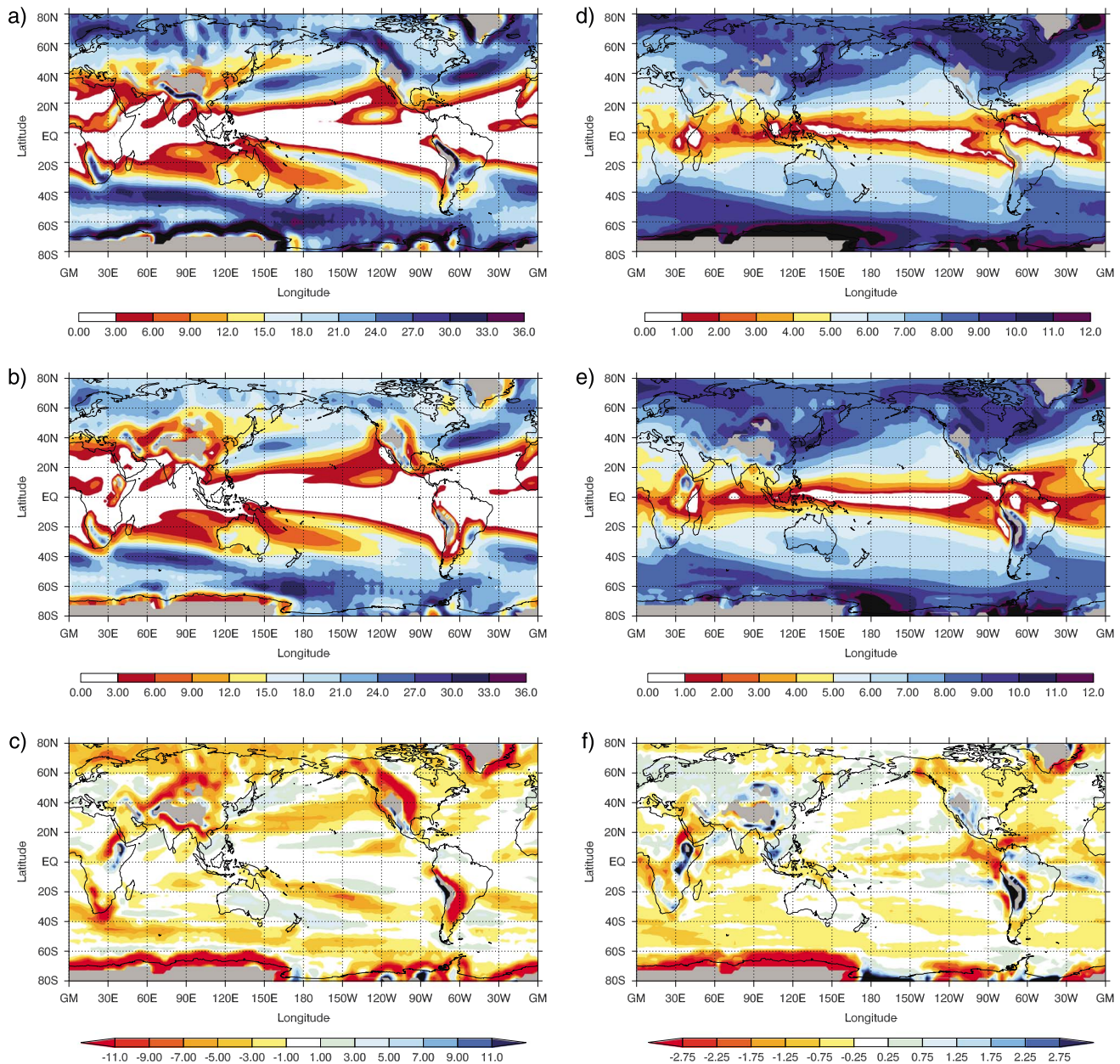


Figure 1. Front frequency for (a) ERA-Interim (1980–2005), (b) multimodel mean for historical simulation (1980–2005), and (c) the multimodel mean bias (models minus ERA-Interim) (%; 1980–2005). Front strength for (d) ERA-Interim, (e) multimodel mean historical simulations, and (f) the multimodel mean bias (models minus ERA-Interim) (10^{-5} K/100 km). Topography above the 850 hPa level is masked out in grey.

24%. In the SH there are maxima stretching eastward and poleward in tilted bands from the east of South America, and the cape of South Africa, with frequencies over 30%. There is also a large maximum at around 60°S. Again, this is a very similar structure to that seen in ERA-Interim. Looking at the difference between the multimodel mean and the ERA-Interim front frequency (Figure 1c), we can see that the average front frequency is quite well represented by the multimodel mean. There is generally a poleward bias in the front frequency maximum in the NH midlatitude storm track regions, particularly in the North Pacific where there is a negative bias of about 5% at 30°N, and a positive bias of the same magnitude at around 45°N. The multimodel mean does not capture the high frequency of fronts observed in the South Pacific Convergence Zone (SPCZ) region. This is likely associated with the models' difficulties in capturing the SPCZ rainfall variability [Brown *et al.*, 2013]. There is also a positive bias across Australia and eastward across the north of

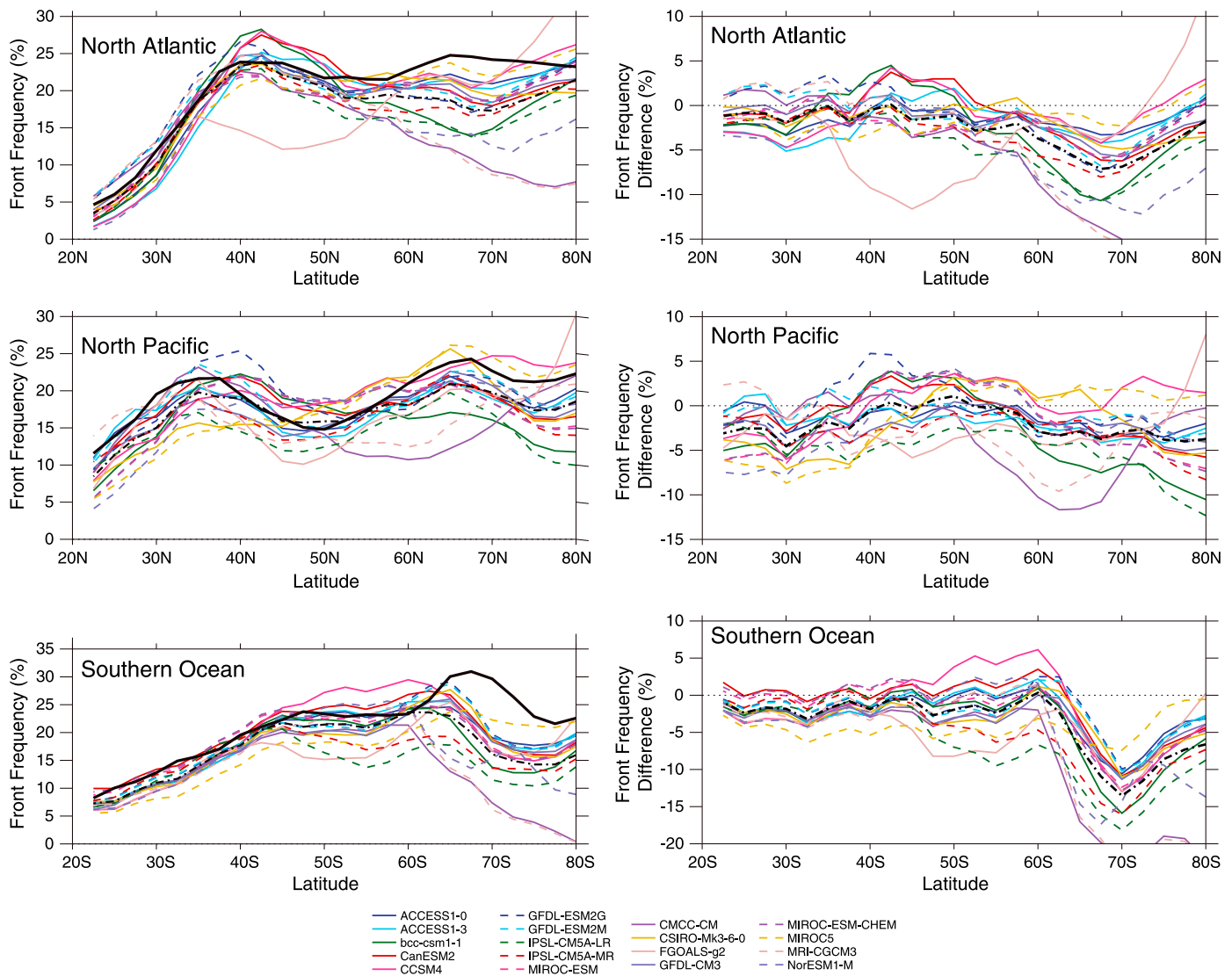


Figure 2. (left) Zonal mean front frequency (% time a front is present in a grid box) and (right) absolute difference between historical CMIP5 simulations and ERA-Interim for the three regions: North Atlantic, North Pacific, and Southern Ocean. The heavy black solid line in the left figure shows the ERA-Interim zonal mean, and the black heavy dashed line represents the multimodel mean.

New Zealand of up to 9%. The large negative biases around regions of high orography, for example, around Antarctica and Greenland, are associated with the different handling of data around regions of orography above the 850 hPa level in the models and the reanalysis, and are an artifact of the front identification. The multimodel mean and the individual models are also capable of capturing the seasonal changes in front frequency (Figures S1 and S2 in the supporting information).

Figure 2 shows the zonal mean front frequency for the individual models considered and the differences between the models and ERA-Interim for the three different storm track regions. The multimodel mean zonal average is also shown for each region. Figure 2 shows that while the multimodel mean front frequency bias is small in all the regions, this represents the average of a range of biases. In the North Atlantic, some of the models have positive biases at most latitudes (e.g., Geophysical Fluid Dynamics Laboratory-Earth System Model (GFDL-ESM2G)), one model has a strong negative bias in the midlatitudes (Flexible Global Ocean-Atmosphere-Land System (FGOALS-g2)), while others show poleward shifts in the front locations (e.g., Community Climate System Model (CCSM4)), as seen by the negative bias around 30°N and the positive bias between 40°N and 60°N. In the North Pacific, although there is a range in the magnitude of

the biases, most of the models show a negative bias between 20°N and 35°N and positive biases further north, representing a shift in the front locations as seen in the multimodel mean maps (Figure 1b). Over the Southern Ocean storm track many of the models have similar biases, with most underestimating the front frequency between 20°S and 40°S. From 40°S to 60°S the models diverge in their representation of the front frequency, leading to a small multimodel mean bias. Poleward of 60°S, there are large negative biases in the zonal mean, which are indicative of the different considerations of orography around Antarctica. The biases in the models are very similar when considering the seasons separately (Figure S3 in the supporting information).

The front strength for ERA-Interim, the multimodel mean, and the difference between the multimodel mean and ERA-Interim are shown in Figures 1d–1f, respectively. In ERA-Interim, the maximum front strength is seen on the western edges of the NH storm tracks, where there are strong thermal contrasts between the land and ocean. In the SH the fronts generally become stronger toward the poles, but there is a local maximum in the eastern Pacific Ocean, to the east of the Andes, and a region of stronger fronts over the south of Australia. The overall spatial distribution and magnitude of the front strength looks very similar in the multimodel mean (Figure 1e).

Comparing the front strength from the multimodel mean with ERA-Interim (Figure 1f) shows that the models do a very good job of representing the front strength since the differences are small in most places. The models show that they have stronger fronts in the highest latitudes and most eastern parts of the NH storm tracks. They underestimate the strength of the fronts in the Indian Ocean region (where they also show a lower front frequency). The average strength of the fronts from each model does not depend on the original horizontal resolution of the model (not shown), consistent with the findings of Mizuta [2012] that the storm track density bias is not resolution dependent.

4. Future Projections

Figure 3a shows the multimodel mean front frequency from the RCP8.5 simulations. We see that the major features of the present day are still visible, with the NH and SH storm tracks over the major ocean basins. The difference in front frequency between the RCP8.5 and historical simulations shown in Figure 3b indicate that there are some changes in the future projections. In the North Atlantic region there is a tripole pattern of change with a strong decrease in front frequency over the Gulf Stream, a weaker increase around 45°N–50°N and a strong decrease further north. The increase lies on the poleward side of the front frequency maximum seen in the historical simulations (Figure 1b), and the lower latitude decrease is on the equatorward side. This indicates a poleward shift of the region of maximum front frequency along with an overall decrease in front frequency. The poleward shift is consistent with the findings of Zappa *et al.* [2013b] for the changes in the North Atlantic and European storm tracks. The strong decrease at higher latitudes can be explained by the strong reduction in the meridional temperature gradient in the region (Figure 3e), with relatively low values of warming in the eastern North Atlantic basin and relatively much higher warming further poleward associated with the Arctic amplification of warming. Over the North Pacific and Asia there is a decrease in front frequency of up to 3%. In the central North Pacific, the minimum decrease in front frequency is on the poleward side of the front frequency maximum, with a very strong decrease on the equatorward side. This is suggestive of a poleward shift combined with a strong reduction, again, associated with the decrease in meridional temperature gradient.

In the SH, over most of the midlatitudes (between 40°S and 60°S) and over Australia, there is an increase in front frequency. This is a region where the multimodel mean change in temperature gradient is positive (Figure 3e). In the Indian Ocean sector of the Southern Ocean, this change represents a poleward shift in the maximum front frequency. Over the eastern Pacific sector of the Southern Ocean, the pattern is more complicated. There appears to be a tripole pattern with a strong decrease in front frequency between 20°S and 40°S, an increase between 40°S and 60°S, and a decrease poleward of that toward the Antarctic continent. Rather than a poleward shift, this represents a concentration of the fronts in the band between 40°S and 60°S. Brown *et al.* [2013] found a projected drying in the RCP8.5 scenario in the SPCZ region which coincides with the decrease in front frequency between 20°S and 40°S. The reduction in front frequency close to Antarctica might be associated with a projected decrease in the sea ice in the region [Collins *et al.*, 2013], and the relative weaker temperature gradients being identified in the region. In both hemispheres

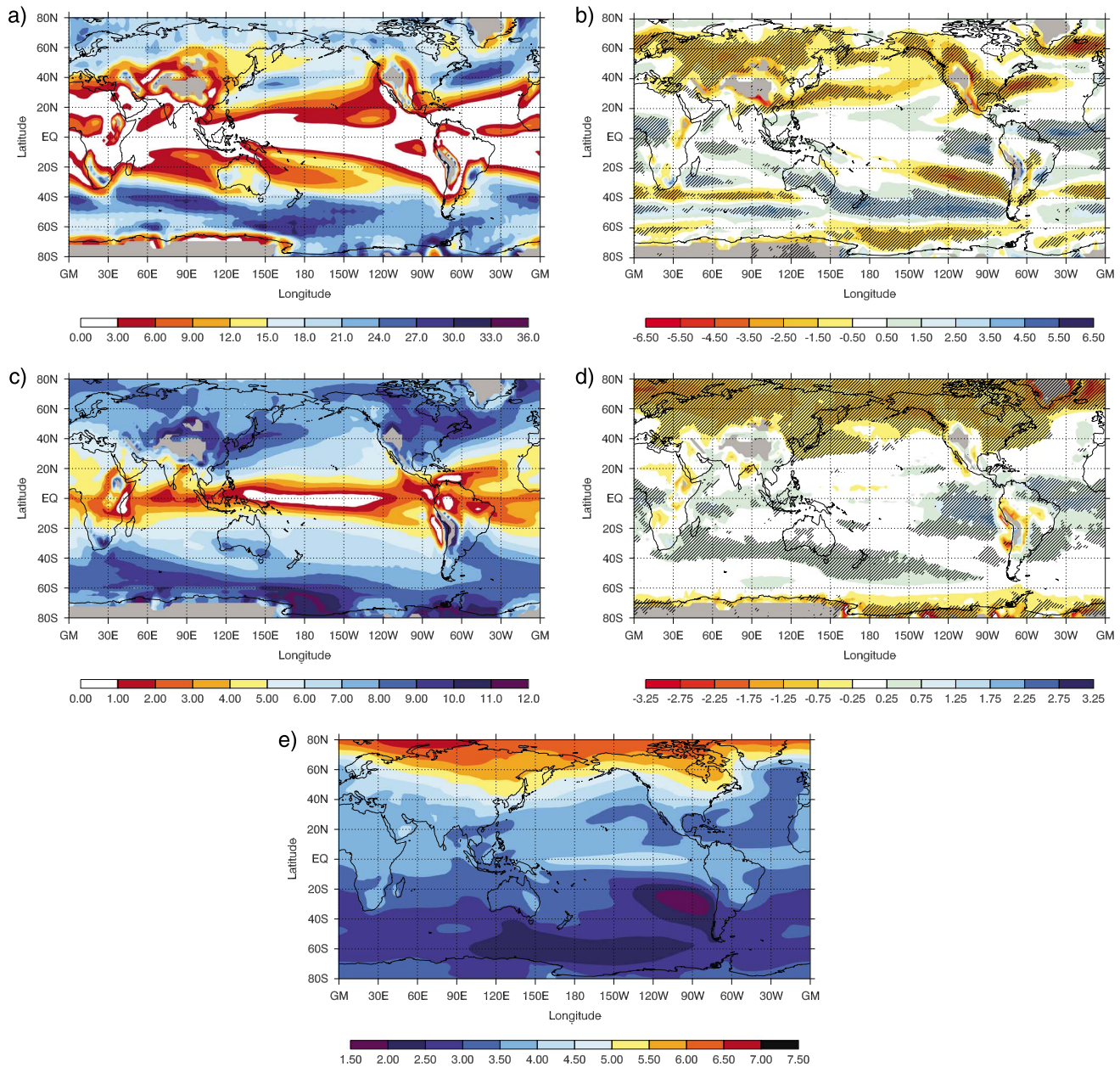


Figure 3. Front frequency for (a) multimodel mean from RCP8.5 simulations and multimodel mean change front frequency (%; RCP8.5 2080–2100—Historical 1980–2005) and front strength for (c) multimodel mean and (d) multimodel mean change (K/100 km; RCP8.5 2080–2100—Historical 1980–2005). Topography above the 850 hPa level is masked out in grey. Multimodel mean 850 hPa wet-bulb potential temperature change (e) between RCP8.5 and historical simulations (K). Hatching in Figures 3b and 3d shows where at least 15 out of 18 models agree in the sign of change.

there is good model agreement, with at least 15 out of the 18 models agreeing on the sign of the changes where the changes are large (Figure 3b).

Figure 4 shows the zonal percentage change in the frequency of fronts over the different storm track regions in the RCP8.5 scenario versus the historical scenario for each of the models. The tripole pattern of change in the North Atlantic region can be seen with strong decreases in front frequency in most models around 35°N and 60°N. In the North Pacific region most of the models exhibit decreases in front frequency of up to 20%, but the models vary quite a lot. In the Southern Ocean region all models show an increase in front frequency at around 50°S with varying magnitudes (up to a 40% increase in GFDL-CM3 (Climate Model version 3)). The largest changes are seen during December, January, and February (DJF) in all ocean basins (Figure S4 in the supporting information).

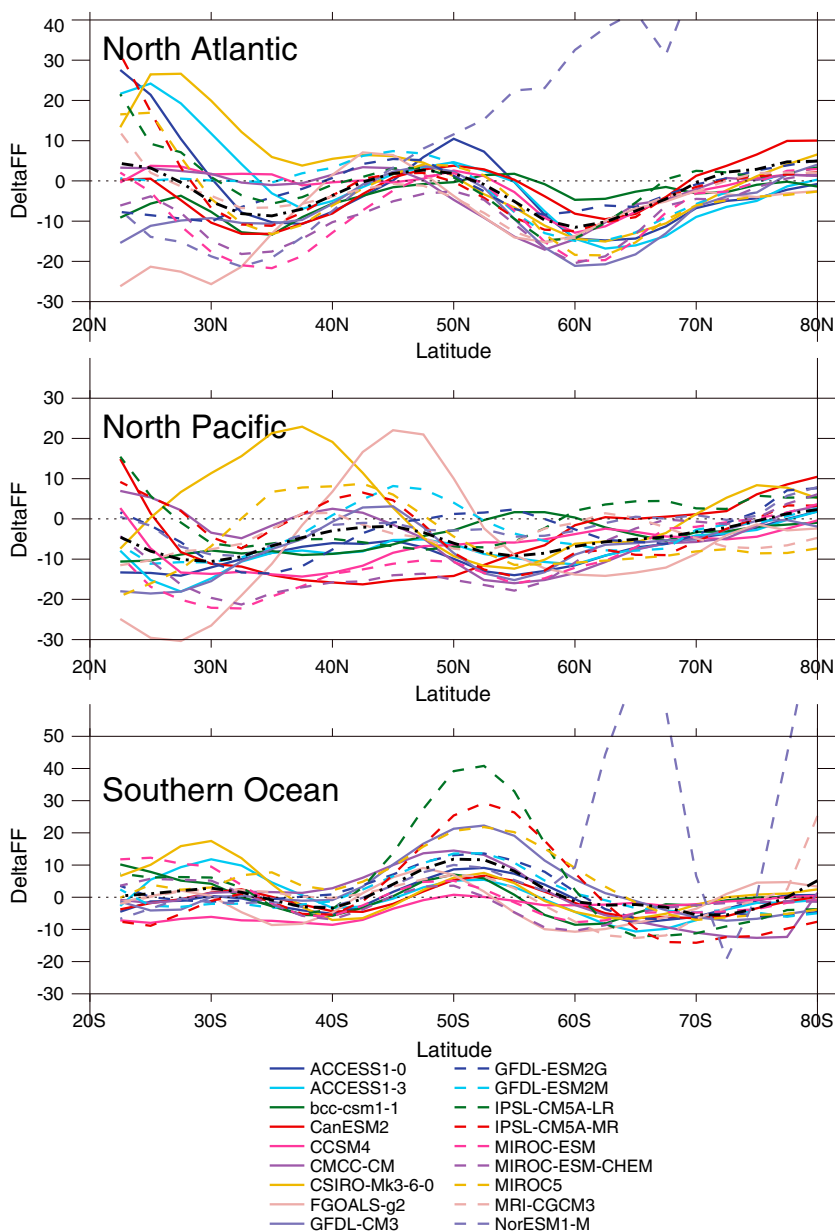


Figure 4. Zonal mean relative difference between RCP8.5 and Historical simulations for front frequency ($\Delta FF = (RCP8.5 - \text{historical}) / \text{historical}$, %). The black heavy dashed line represents the multimodel mean change.

The front strength in the RCP8.5 multimodel mean is shown in Figure 3c, and the difference between the RCP8.5 and the historical simulations is shown in Figure 3d. Over most of the NH, there is a decrease in the front strength with a local maximum of around 1.5 K/100 km (a decrease of over 15%) over the coast of Alaska and a larger maximum of around 2.5 K/100 km (a decrease of over 25%) over the Greenland Sea. In general, the front strength decreases more toward the higher latitudes. This reduction in front strength is consistent with the amplified surface warming at the high latitudes in the NH reducing the meridional temperature gradient.

In the tropical Atlantic and eastern Pacific there is an increase in front strength coinciding with the increase in front frequency; however, there are very few fronts in this region generally. Over the SH midlatitudes, there are very small changes in front strength, with an increase over the Southern Ocean of around 0.5 K/100 km. Around the edge of Antarctica there is a decrease in the front strength, likely associated with

the sea ice reductions in this region. Again, there is good model agreement on the sign of the changes suggesting these results are robust (Figure 3d).

5. Summary and Discussion

We have applied an automated front identification methodology based on the work of *Hewson* [1998] and *Berry et al.* [2011a] to a number of models from the CMIP5 database. We calculated the front frequency (as the percentage of days a front is present in a grid box) and the front strength from the historical and RCP8.5 simulations from each of the models listed in Table S1.

The biases in the multimodel mean front frequency are found to be similar to the single-model results of *Catto et al.* [2013]. The models exhibit a poleward bias in the maximum front frequency in the North Pacific Ocean region, relatively small biases in the North Atlantic, too few fronts over the SPCZ and Southern Ocean regions, and slightly too many over Australia and New Zealand. The front strength is fairly well represented in the models. In the RCP8.5 scenario, the North Pacific exhibits a decrease in front frequency along with decreases in the front strength consistent with the weakening meridional temperature gradient in the region. The North Atlantic region shows a tripole pattern of change with decreases in front frequency equatorward of the maximum, increases on the poleward edge of the maximum, and decreases further poleward. This is consistent with the pattern of extratropical storm track changes seen by *Zappa et al.* [2013b]. In most of the SH the shift in front frequency is poleward, consistent with the general view of the midlatitude storm tracks moving poleward and clearly shown by the zonal mean change. Using a different front identification method may give different quantitative results, but the consistency of our results with those from storm track studies suggests this difference would be small.

Here we have used only one warming scenario from the CMIP5 database, the most extreme scenario. Previous studies have shown that the North Atlantic storm tracks in particular do not show linear changes with increasing forcing [*Catto et al.*, 2011], so the changes seen here in the fronts may exhibit different patterns in other scenarios. However, the changes shown in the SH are similar to a number of studies all showing a poleward shift in the storm tracks [e.g., *Grieger et al.*, 2014; *Chang et al.*, 2013].

In the present study, the threshold of the thermal front parameter used for the front identification given in *Berry et al.* [2011a] has been used for the identification of the fronts in ERA-Interim and both the historical and future simulations. This has allowed a like-for-like comparison between the different data sets. Since we find that there is a weakening of fronts in the future simulations, we might consider that a different threshold could be used. We have investigated this by calculating the average thermal front parameter between 60°S and 60°N and 180°E and 150°W (to eliminate the effect of any orography) and over all years for each of the data sets. The values from the models range from around $5.5 \times 10^{-12} \text{ km}^{-2}$ to $6.6 \times 10^{-12} \text{ km}^{-2}$, all lying within the interannual standard deviation of the ERA-Interim value of $6 \times 10^{-12} \text{ km}^{-2}$. There is no systematic difference between the historical and the RCP8.5 simulations with some models showing an increase in the future simulations, and others showing a decrease. This suggests that while locally there are changes in the thermal gradients, leading to the detection of fewer fronts in the North Pacific region for example, on the large scale there is no difference. The use of the same threshold value is therefore justified, and the results shown here give a broad idea of how fronts are represented in climate models, and how their frequency might change in the future.

A key remaining question is how the precipitation associated with the fronts may change in a warming climate, and how this relates to the front strength shown here. Studies have shown that precipitation associated with cyclones may increase in future warming scenarios [*Champion et al.*, 2011; *Zappa et al.*, 2013b] so it could be expected that the fronts will exhibit the same changes. This question will be addressed in a future paper.

References

- Berry, G., M. J. Reeder, and C. Jakob (2011a), A global climatology of atmospheric fronts, *Geophys. Res. Lett.*, *38*, L04809, doi:10.1029/2010GL046451.
- Berry, G., C. Jakob, and M. J. Reeder (2011b), Recent global trends in atmospheric fronts, *Geophys. Res. Lett.*, *38*, L21812, doi:10.1029/2011GL049481.
- Bi, D., et al. (2013), The ACCESS coupled model: Description, control climate, and evaluation, *Aust. Meteorol. Oceanogr. J.*, *63*, 41–64.
- Bjerknes, J., and H. Solberg (1922), Life cycle of cyclones and the polar front theory of atmospheric circulation, *Geophys. Publ.*, *3*, 1–18.

Acknowledgments

This study was supported by the Australian Research Council through the Linkage Project grants LP0883961 and LP130100373, the Discovery Project grant DP0877417, the ARC Centre of Excellence for Climate System Science grant CE110001028, and the Discovery Early Career Researcher Award grant DE140101305. The front identification algorithm was kindly provided by Gareth Berry. We acknowledge the World Climate Research Programme's Working Group on Coupled Modelling, which is responsible for CMIP, and we thank the climate modeling groups (listed in Table S1 in the supporting information of this paper) for producing and making available their model output. For CMIP the U.S. Department of Energy's Program for Climate Model Diagnosis and Intercomparison provides coordinating support and led development of software infrastructure in partnership with the Global Organization for Earth System Science Portals. CMIP5 data are available from <http://pcmdi9.llnl.gov/esgf-web-fe/>, and ERA-Interim data are available from <http://apps.ecmwf.int/datasets/>. J.L.C. would also like to thank Harvey Ye for all his help downloading the CMIP5 data.

Noah Diffenbaugh thanks two anonymous reviewers for their assistance in evaluating this paper.

- Brown, J. R., A. F. Moise, and R. A. Colman (2013), The South Pacific Convergence Zone in CMIP5 simulations of historical and future climate, *Clim. Dyn.*, *41*, 2179–2197, doi:10.1007/s00382-012-1591-x.
- Browning, K. A., and G. A. Monk (1982), A simple model for the synoptic analysis of cold fronts, *Q. J. R. Meteorol. Soc.*, *108*, 435–452.
- Catto, J. L., and S. Pfahl (2013), The importance of fronts for extreme precipitation, *J. Geophys. Res. Atmos.*, *118*, 10,791–10,801, doi:10.1002/jgrd.50852.
- Catto, J. L., L. C. Shaffrey, and K. I. Hodges (2011), Northern Hemisphere extratropical cyclones in a warming climate in the HiGEM high-resolution climate model, *J. Clim.*, *24*, 5336–5352, doi:10.1175/2011JCLI4181.1.
- Catto, J. L., C. Jakob, G. Berry, and N. Nicholls (2012), Relating global precipitation to atmospheric fronts, *Geophys. Res. Lett.*, *39*, L10805, doi:10.1029/2012GL051736.
- Catto, J. L., C. Jakob, and N. Nicholls (2013), A global evaluation of fronts and precipitation in the ACCESS model, *Aust. Meteorol. Oceanogr. J.*, *63*, 191–203.
- Champion, A. J., K. I. Hodges, L. O. Bengtsson, N. S. Keenlyside, and M. Esch (2011), Impact of increasing resolution and a warmer climate on extreme weather from Northern Hemisphere extratropical cyclones, *Tellus A*, *63*, 893–906.
- Chang, E. K. M., Y. J. Gao, X. M. Xia, and M. H. Zheng (2013), Storm-track activity in IPCC AR4/CMIP3 model simulations, *J. Clim.*, *26*, 246–260, doi:10.1175/JCLI-D-11-00707.1.
- Colle, B. A., Z. Zhang, K. A. Lombardo, E. Chang, P. Liu, and M. Zhang (2013), Historical evaluation and future prediction of eastern North American and western Atlantic extratropical cyclones in the CMIP5 models during the cool season, *J. Clim.*, *26*, 6882–6903, doi:10.1175/JCLI-D-12-00498.1.
- Collins, M., et al. (2013), Long-term climate change: Projections, commitments and irreversibility, in *Climate Change 2013: The Physical Science Basis. Contribution of Working Group I to the Fifth Assessment Report of the Intergovernmental Panel on Climate Change*, edited by T. F. Stocker et al., pp. 1029–1136, Cambridge Univ. Press, Cambridge, U. K., and New York.
- Dee, D. P., et al. (2011), The ERA-Interim reanalysis: Configuration and performance of the data assimilation system, *Q. J. R. Meteorol. Soc.*, *137*, 553–597.
- Grieger, J., G. C. Leckebusch, M. G. Donat, M. Schuster, and U. Ulbrich (2014), Southern Hemisphere winter cyclone activity under recent and future climate conditions in multi-model AOGCM simulations, *Int. J. Climatol.*, *34*, 3400–3416, doi:10.1002/joc.3917.
- Hewson, T. D. (1998), Objective fronts, *Meteorol. Appl.*, *5*, 37–65.
- Hope, P., K. Keay, M. Pook, J. L. Catto, I. Simmonds, G. Mills, P. McIntosh, J. Risbey, and G. Berry (2014), A comparison of automated methods of front recognition for climate studies—A case study in south west Western Australia, *Mon. Weather Rev.*, *142*, 343–363.
- Joly, A., et al. (1999), Overview of the field phase of the fronts and Atlantic storm-track experiment (FASTEX) project, *Q. J. R. Meteorol. Soc.*, *125*, 3131–3163.
- Mizuta, R. (2012), Intensification of extratropical cyclones associated with the polar jet change in the CMIP5 global warming projections, *Geophys. Res. Lett.*, *39*, L19707, doi:10.1029/2012GL053032.
- Neu, U., et al. (2013), IMILAST: A community effort to intercompare extratropical cyclone detection and tracking algorithms, *Bull. Am. Meteorol. Soc.*, *94*, 529–547, doi:10.1175/BAMS-D-11-00154.1.
- Pitt, M. (2008), The Pitt review—Lessons learned from the 2007 summer floods, *Final Rep.*, Cabinet Office, London, U. K.
- Pook, M. J., P. C. McIntosh, and G. A. Meyers (2006), The synoptic decomposition of cool-season rainfall in the southeastern Australian cropping region, *J. Appl. Meteorol. Climatol.*, *45*, 1156–1170.
- Pook, M. J., J. S. Risbey, and P. C. McIntosh (2012), The synoptic climatology of cool-season rainfall in the Central Wheatbelt of Western Australia, *Mon. Weather Rev.*, *140*, 28–43.
- Renard, R. J., and L. C. Clarke (1965), Experiments in numerical objective frontal analysis, *Mon. Weather Rev.*, *93*, 547–556.
- Simmonds, I., K. Keay, and J. A. T. Bye (2011), Identification and climatology of Southern Hemisphere mobile fronts in a modern reanalysis, *J. Clim.*, *25*, 1945–1962.
- Taylor, K. E., R. J. Stouffer, and G. A. Meehl (2012), An overview of CMIP5 and the experiment design, *Bull. Am. Meteorol. Soc.*, *93*, 485–498, doi:10.1175/BAMS-D-11-00094.1.
- Ulbrich, U., et al. (2013), Are greenhouse gas signals of Northern Hemisphere winter extra-tropical cyclone activity dependent on the identification and tracking algorithm?, *Meteorol. Z.*, *22*(1), 61–68.
- Woollings, T., J. M. Gregory, J. G. Pinto, M. Reyers, and D. J. Brayshaw (2012), Response of the North Atlantic storm track to climate change shaped by ocean-atmosphere coupling, *Nat. Geosci.*, *5*, 313–317.
- Zappa, G., L. C. Shaffrey, and K. I. Hodges (2013a), The ability of CMIP5 models to simulate North Atlantic extratropical cyclones, *J. Clim.*, *26*, 5379–5396, doi:10.1175/JCLI-D-12-00501.1.
- Zappa, G., L. C. Shaffrey, K. I. Hodges, P. G. Sansom, and D. B. Stephenson (2013b), A multimodel assessment of future projections of North Atlantic and European extratropical cyclones in the CMIP5 climate models, *J. Clim.*, *26*, 5846–5862, doi:10.1175/JCLI-D-12-00573.1.